Nanoscale Res Lett (2010) 5:1111–1117
DOI 10.1007/s11671-010-9610-5

NANO EXPRESS

Effect of Crystallographic Texture on Magnetic Characteristics of Cobalt Nanowires

K. Maaz · S. Karim · M. Usman · A. Mumtaz · J. Liu · J. L. Duan · M. Maqbool

Received: 15 February 2010 / Accepted: 9 April 2010 / Published online: 23 April 2010

Abstract Cobalt nanowires with controlled diameters have been synthesized using electrochemical deposition in etched ion-track polycarbonate membranes. Structural characterization of these nanowires with diameter 70, 90, 120 nm and length 30 μm was performed by scanning electron microscopy, high-resolution transmission electron microscopy, and X-ray diffraction techniques. The as-prepared wires show uniform diameter along the whole length and X-ray diffraction analysis reveals that [002] texture of these wires become more pronounced as diameter is reduced. Magnetic characterization of the nanowires shows a clear difference of squareness and coercivity between parallel and perpendicular orientations of the wires with respect to the applied field direction. In case of parallel applied field, the coercivity has been found to be decreasing with increasing diameter of the wires while in perpendicular case; the coercivity observes lower values for larger diameter. The results are explained by taking into account the magnetocrystalline and shape anisotropies with respect to the applied field and domain transformation mechanism when single domain limit is surpassed.

K. Maaz (✉) · S. Karim
Physics Division, PINSTECH, P.O. Nilore, Islamabad, Pakistan
e-mail: maaz@impcas.ac.cn

M. Usman · A. Mumtaz
Department of Physics, Quaid-i-Azam University, Islamabad, Pakistan

J. Liu · J. L. Duan
Institute of Modern Physics, Chinese Academy of Sciences, Lanzhou, People's Republic of China

M. Maqbool
Department of Physics and Astronomy, Ball State University, Muncie, IN 47306, USA

Keywords Co nanowires · Electrodeposition · Magnetic properties

Introduction

Nanostructured materials are the subject of immense interest because of their interesting electrical, optical, mechanical, chemical, and magnetic properties [1–7]. Fabrication and characterization of magnetic nanowires are of particular interest from both fundamental research and technological point of views. The interest in magnetic nanowires emerges due to their enhanced and novel properties when compared to their bulk counterparts that lead to potential applications in future high density magnetic devices and sensors, etc. [6, 8–11].

Cobalt is a well-known hard magnetic material and its compounds are widely used for variety of applications in computer, electronic, and medical industries [6, 9, 11]. It is one of the most interesting magnetic materials due to its large magnetocrystalline anisotropy that lies along the c-axis. Various parameters including shape, size, and texture strongly influence magnetic properties of cobalt nanowires. These parameters can be controlled during fabrication process, for example, fcc phase of cobalt nanowires can be changed to hcp phase only by varying pH of the solution during fabrication [12]. Strijkers et al. [13] have reported that the easy axis of magnetization can be tuned either perpendicular or parallel to the wire long axis by changing the length of wires. The influence of current density and wires' diameter on magnetic properties is also documented in the literature [14–17].

In this work, arrays of cobalt nanowires have been fabricated by electrochemical deposition in porous

polycarbonate membranes. This method is a versatile and suitable approach for large-scale production of nanowires with well-defined shape and crystallinity that are important for future applications [18–21]. This technique allows to independently vary the length, size, geometry and density of wires, making it feasible to investigate the influence of these parameters independently on physico-chemical characteristics. Specifically, in this work, we present a study on how the diameter affects the magnetic properties of Co wires with 70, 90, and 120 nm diameters by influencing the crystallographic texture. The results are explained by taking into account the magnetocrystalline and shape anisotropies with respect to the external applied field and domain transformation mechanism when single domain limit is surpassed.

Experimental Procedure

Polycarbonate foils of thickness 30 μm were irradiated at normal incidence with ^{238}U ions (kinetic energy 11.4 meV/u, fluence 10^8 ions cm^{-2}). While passing through the target, each ion creates a cylindrical damage zone along its trajectory which is further sensitized by UV light exposure for 2 h. The UV exposure enhances the track-etching rate supporting thus the formation of cylindrical tracks in polycarbonate membranes [18, 22]. Subsequently, the foils were etched in 5 M NaOH solution at 50°C to obtain the cylindrical nanochannels. Diameter of the etched pores was controlled by the etching time. Three different diameters 70, 90, and 120 nm were used in this study, which are prepared by etching the samples for different times. In the next step, a thin gold layer (~30 nm thickness) was sputtered onto one side of the membrane and subsequently reinforced by electrochemically deposited copper layer of ~5 micron thickness. This layer served as a cathode during the wires fabrication process, while a cobalt rod was used as an anode. The electrolyte consists of 1 M $CoSO_4 \cdot 7H_2O$ and the initial pH of this solution was adjusted to 6 by adding appropriate amount of H_2SO_4. The deposition of Co was performed using a constant voltage of −1 V at room temperature and electric current was monitored as a function of time. The electrolyte solution and deposition parameters were kept constant during all the experiments.

Morphology of the nanowires was investigated by scanning electron microscopy (SEM, JSM-6700F) and high-resolution transmission electron microscopy (HRTEM, JEM-3010, 300 kV), while composition of the wires was studied by means of energy dispersive X-ray analysis (EDS). For analyzing texture of the nanowires, X-ray diffraction (XRD, X'Pert Pro, Cu-K_α, 1.54056Å) was used. Additionally, magnetic characterization has been performed by quantum design physical property measurement system (PPMS) up to a maximum field of 10 kOe. For SEM and TEM analyses, nanowires were liberated from the template by dissolving the polymer matrix in dichloromethane, on the other hand for magnetic and XRD characterizations the wires were left embedded in the template and Au/Cu substrate layer was removed.

Results and Discussion

Figure 1 displays the current-versus-time curves recorded during electrodeposition of Co wires of diameter 70 nm. The shape of the curves is in agreement with the behavior described previously [23, 24]. Typically, there are three different zones (I, II, and III) as indicated in this figure. Initially when a potential is applied, the current exhibits a sharp increase followed by the rapid decrease that is ascribed to the charge of the electrical double layer (zone-I). During the growth of cobalt nanowires in pores, the current remains nearly constant (zone II) until the wires reach the polymer upper surface. When three-dimensional buds or the so-called caps start to form on the upper surface, the cathode area thus enlarges and therefore the current increases rapidly (zone-III). The deposition was instantly stopped as soon as the deposition current was observed to increase, i.e., zone-III. The caps were removed from the upper surface with the help of adhesive tape for magnetic and XRD analyses.

Figure 2a shows a low magnification SEM micrograph of the as-prepared Co nanowires. Since the wires are magnetic in nature, magnetostatic attractions among the wires causes bunches of nanowires when the polymer is dissolved. High magnification SEM image of Co wires

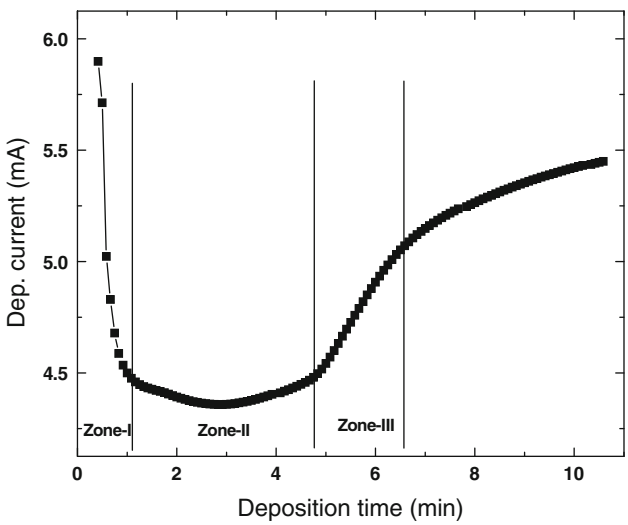

Fig. 1 Experimentally measured deposition current as a function of deposition time recorded during wires synthesis. *Zone-I*, *II*, and *III* are explained in the text

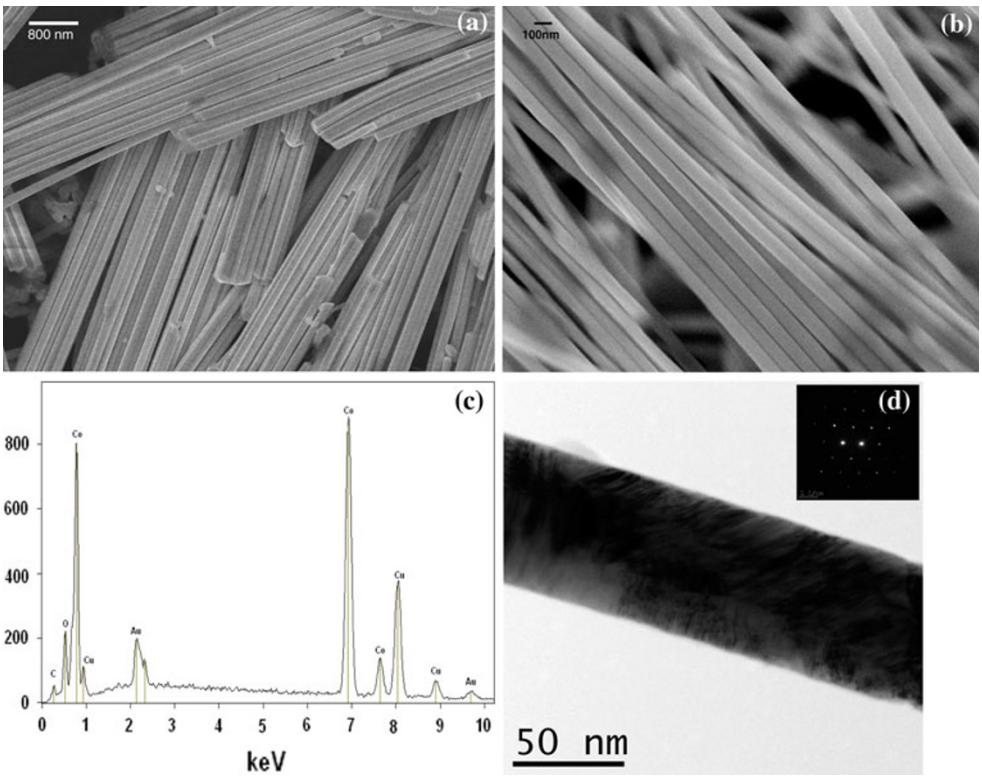

Fig. 2 **a**, **b** SEM micrographs of 120- and 90-nm-diameter cobalt wires, respectively, **c** EDS spectrum of cobalt nanowires. In the pattern, the Cu and Au *peaks* represent the substrate materials, **d** TEM micrograph of a 70-nm-diameter wire and respective SAED pattern (*inset*)

with diameters of ~90 nm is presented in Fig. 2b. These images show that the prepared nanowires are cylindrical in shape with uniform cross-section over their whole length and wires exhibit homogenous contours. Due to the good quality of the polymeric templates used in this work, the diameter distribution within a given sample remains very narrow. Standard deviation in diameters of the wires was less than 5% of the mean values. The characteristics of the membranes employed are extremely important for fabrication of nanowires. Shape of the pores in commercially available membranes is reported to be toothpick- or cigar-like [23, 25]. The origin of such shapes is ascribed to the presence of surfactants in the etching solution [26]. The wires prepared in the commercial membranes are reported to be up to a factor 2.5 wider in the central part than at the ends [23]. By employing an etching solution without additives as well as by treating the membranes with UV light prior to etching in order to increase the track-to-bulk etching ratio, we were able to prepare uniform cylindrical wires. Figure 2c shows the composition analysis of the nanowires performed by EDS. In the figure, the Cu, Co, and Au peaks are present. The Cu and Au signals may originate from the substrate materials used for the production of these nanowires.

Figure 2d shows a TEM micrograph and corresponding selected-area electron diffraction (SAED) pattern (in the inset) of a segment of a randomly selected 70-nm-diameter Co wire. Analysis by TEM confirms the cylindrical morphology and uniform contour of the wires as observed in SEM. In general, no grain boundaries were observed in these nanowires by TEM or in SAED patterns confirming thus that wires consist of at least several micrometers long single crystals.

Figure 3 shows the XRD patterns of Co nanowires of diameters 70, 90, and 120 nm. The diffraction pattern is in agreement with the powder sample (JCPDS 5-727), indicating that the wires possess hcp structure. These results are in agreement with the literature that the structure of Co nanowires is hcp when the pH value of electrolyte is above 3.5 [12, 16]. However, in contrast to the powder diffractogram, the relative intensity of the (002) plane, is significantly larger than other planes, evidencing a preferred crystallographic orientation along the [002] direction. The interesting result is that the reflection from (002) plane is strongest in thinner nanowires (70 nm). To quantitatively investigate the degree of preferred orientations, the texture coefficients (TC) of first three reflections, i.e., (100), (002), (101) are calculated using following equation [27]:

$$TC(hkl)_i = \frac{I(hkl)_i / I_o(hkl)_i}{\frac{1}{N}\sum_n \frac{I(hkl)_n}{I_o(hkl)_n}} \quad (1)$$

where $I(hkl)_i$ is the observed intensity of the $(hkl)_i$ plane, $I_o(hkl)_i$ is the intensity of the $(hkl)_i$ reflection of a polycrystalline sample, N is the total number of reflections taken into account, and (hkl) denotes the Miller indices of

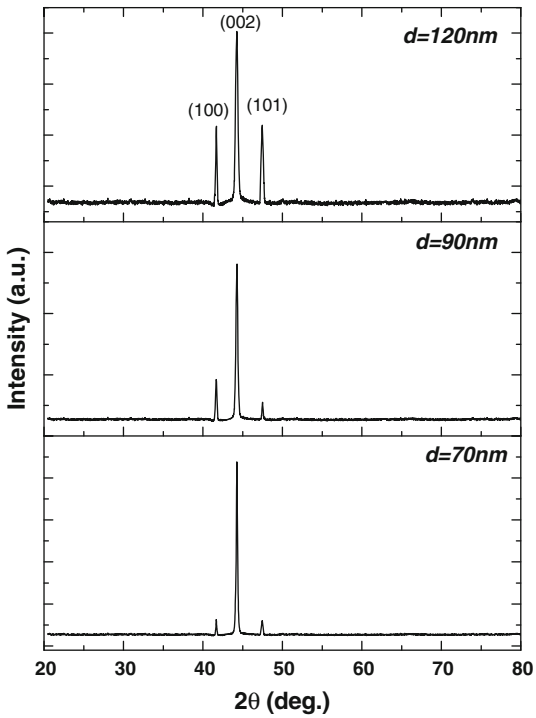

Fig. 3 XRD diffractogram of cobalt nanowires

the lattice planes of a given signal. TC values larger than 1 indicate a preferred orientation of the crystals/grains in the samples. The maximum value of TC is defined by *N*. The calculated results are presented in Table 1.

In the case of $d = 70$ nm, TC_{002} is 1.94 while TC_{100} and TC_{101} are less than 1, indicating that the cobalt nanowires of 70 nm diameter are strongly [002] textured. However, TC_{002} decreases to 1.01 and the values of TC_{100} and TC_{101} increase as the diameter increases from 70 to 120 nm. Thus, the [002] texture diminishes and [100], and [101] texture enhances with increasing diameter. In particular, the gain in TC_{100} is more when compared to TC_{101}. These results are consistent with literature that the diameter of the nanowires influences strongly the texture [18, 28]. The geometrical confinement of small diameter pores favors the growth of single crystals whereas relatively larger pores allows the growth of defects and multi-domain more readily therefore decreasing the texture. In addition, pores with large diameters lead to high current density during electrodeposition. This involves smaller ad-atom mobility and thus a less distinct wire texture [18].

On the other hand, according to Darques et al. [15] wire diameter plays an important role in the final preferred texture also by inducing local changes of the pH within the pores. They distinguished between "local pH" and "solution pH", the pH inside the pores (local pH) is higher than the pH in the solution outside the pores (solution pH) and this difference increases as the pore diameter decreases. It is suggested in reference [15] that an increasing proportion

Table 1 Texture coefficients of (100), (002), and (101) planes for cobalt wires of diameter 70, 90, and 120 nm, respectively

Diameter	TC_{100}	TC_{002}	TC_{101}
70	0.89	1.94	0.16
90	1.39	1.43	0.17
120	1.66	1.01	0.33

of trapped hydrogen bubbles in smaller pores lead to high OH^- ions that increases pH in these pores, which can influence the orientation of crystal planes.

Magnetic hysteresis loops M(H) of the embedded cobalt nanowires have been measured with applied field both parallel and perpendicular to the wire long axis. In case of parallel direction, the M(H) loops are shown in Fig. 4a, c, e for $d = 70$, 90 and 120 nm, respectively, while Fig. 4b, d, f show the loops taken in the case of the field applied perpendicular to the long axis. Squared shape loops in Fig. 4a, c, e show that the resultant anisotropy direction is along the length of the wires when the field was applied parallel to the wire direction. When the field was applied perpendicular to the long wire axis, both coercivity and squareness were found smaller than the parallel case, indicating that the direction of resultant anisotropy lies at certain angle to the wire long axis. It is to be noted that according to Stoner–Wohlfarth's model ($H_C = 2\ K/Ms$) the coercivity is directly proportional to anisotropy for ferromagnetic systems [29, 30]. Where H_C is coercivity, K is anisotropy constant and Ms is the saturation magnetization of the system. The coercivity values calculated from these loops are plotted as a function of wire diameter as given in Fig. 4g, h. In case of field applied parallel to the long axis, the coercivity increases with diminishing wire diameter while in the case of perpendicular field the coercivity at $d = 90$ nm is larger than at $d = 70$ and 120 nm.

To explain diameter-dependent coercivity of nanowires, we consider a schematic diagram indicating the directions of wire long axis, shape and the magnetocrystalline anisotropies for three different textures; [100], [101], and [002] as shown in Fig. 5. In case of bulk hcp cobalt, the magnetocrystalline anisotropy energy density, $K_1 = 5 \times 10^6$ erg cm^{-3} is comparable to the shape anisotropy energy density, $\pi M_s^2 = 6 \times 10^6$ erg cm^{-3} [31]. These values are given for the sake of comparison by assuming that these are valid for cobalt nanowires as well. Therefore, the effective magnetic anisotropy is mainly determined by competition between shape and magnetocrystalline anisotropies. Other anisotropies like rotational, surface and magnetoelastic may be neglected due to their small contribution when compared to shape and magnetocrystalline anisotropies. For high aspect ratio cobalt nanowires, the shape anisotropy is along the long axis of wires; therefore,

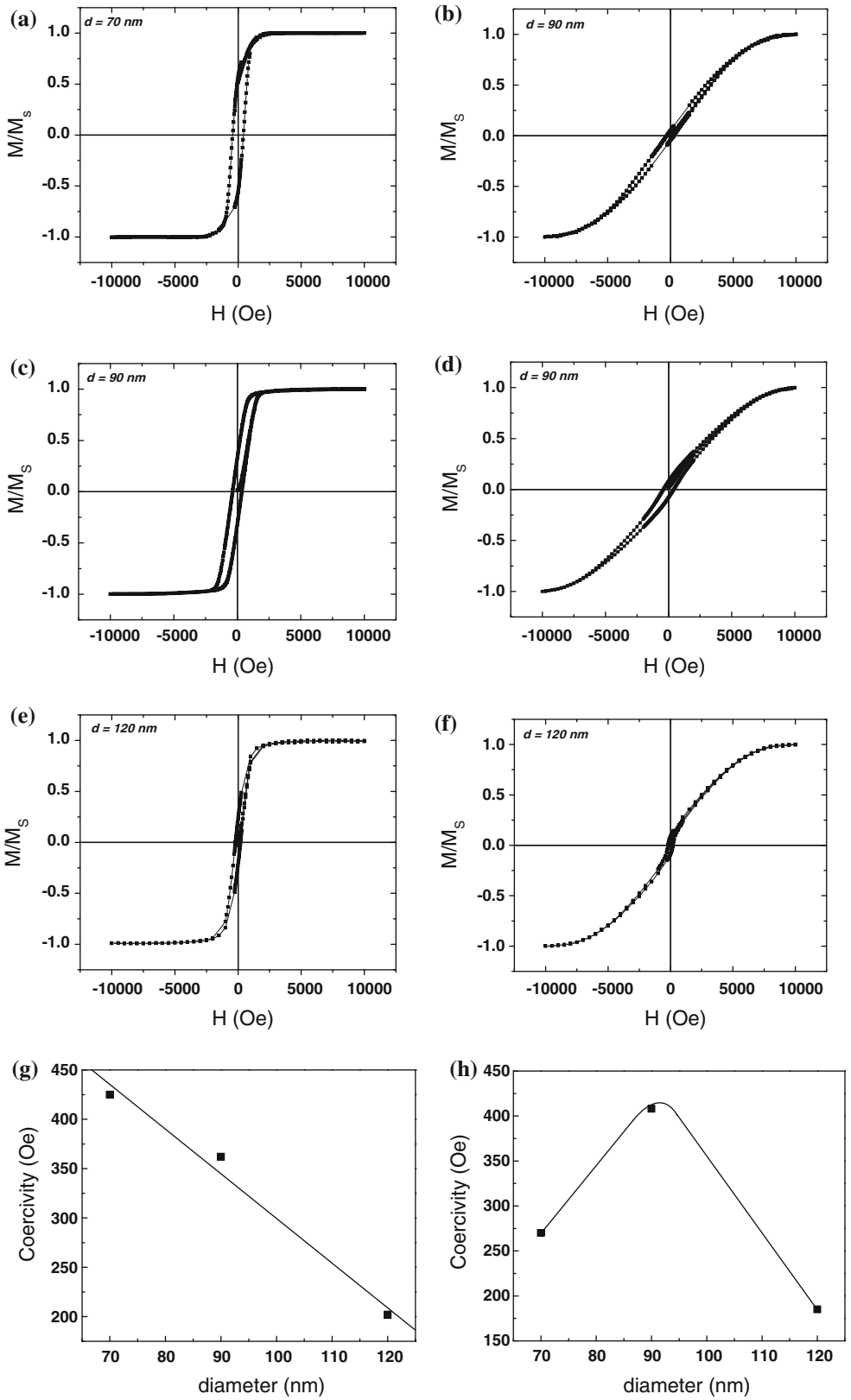

Fig. 4 Comparison of hysteresis loops of cobalt nanowires. **a**, **c**, **e** The loops taken when the magnetic field was applied parallel to the wire long axis, **b**, **d**, **f** The loops taken when the field was applied perpendicular to the wire long axis. **g**, **h** Coercivity values as a function of diameter (calculated from hysteresis loops) for applied filed parallel and perpendicular to the wire long axis, respectively

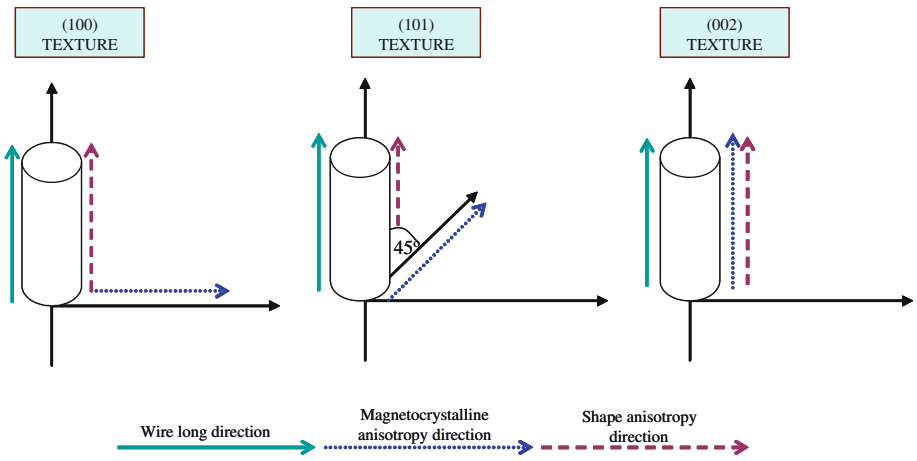

Fig. 5 Schematic diagram showing directions of shape and magnetocrystalline anisotropies and wire long axis for [100], [101], and [002] textures

magnetocrystalline anisotropy is an important factor in determining magnetic properties of the wires.

It has been reported earlier that in hcp cobalt, the direction of easy axis of magnetization (i.e., magnetocrystalline anisotropy) is parallel to wire long axis in case of [002] texture, perpendicular in case of [100] texture and at an angle of 45° in case of [101] texture as shown in schematic diagram (Fig. 5) [16]. Thus, in [002] texture, the directions of shape and crystalline anisotropies are parallel and reinforcing each other that resultantly increases the coercivity of nanowires [16, 32]. From the XRD diffractogram depicted in Fig. 4, [002] texture increases with decreasing diameter therefore when the field was applied parallel to the long axis, the coercivity increases with decreasing diameter and maximum value was observed at $d = 70$ nm (Fig. 4g).

When the field was applied perpendicular to wire long axis the coercivity increases with increasing wire diameter from 70 to 90 nm and then decreases for $d = 120$ nm (Fig. 4 h). The increase in coercivity with diameter is due to the rise in [100] texture with diameter that favors the coercivity in perpendicular direction. However, this increasing trend of coercivity is not continued for large diameter wires (i.e., for 120 nm). For such wires, the appearance of magnetic multi-domains may come into play their role; therefore, the resultant coercivity arises from the two competing mechanisms, namely, the effect of increasing [100] texture (that favors the coercivity) and the domain transformation from single domain to multi-domain region when diameter of the wires surpasses critical size of single domain that reduces the coercivity of thicker nanowires. The later effect (domain transformation) is probably more dominant here that resultantly decreases the net coercivity of 120 nm nanowires [12, 16, 17, 33].

It is worthy to note that in case of perpendicular applied field, coercivity is smaller than the parallel case, particularly for diameter 70 nm. For parallel applied field, strong [002] texture in 70-nm-diameter wires means that magnetocrystalline anisotropy augments the shape anisotropy thereby increasing the effective anisotropy and hence the coercivity (refer to the Fig. 5). However, when field is applied perpendicular to the wire axis, due to strong [002] texture (with anisotropy along the parallel direction) it is difficult for the spins (moments) to align in perpendicular direction (i.e., along the hard axis) as both directions of shape anisotropy and magnetocrystalline anisotropy are pointing to the wire long axis. This resultantly decreases the coercivity in this case.

Conclusion

Cobalt nanowires of diameter 70, 90, and 120 nm have been fabricated by electrodeposition in polycarbonate templates. Structural analysis of the wires confirms the formation of pure phase hcp cobalt nanowires with narrow size distribution. XRD studies of the samples reveal that 70-nm-diameter wires are strongly [002] textured, however, with increasing diameter, [100] and [101] textures also become strong. Coercivity of the nanowires along the wire long axis decreases with increasing diameter most probably due to the effect of decreasing [002] texture that favors the coercivity in a direction parallel to the wire long axis. In perpendicular case, the coercivity was found to increase with increasing diameter due the increasing [100] and [101] textures and then decreases for 120 nm wire due the dominant role of domain transformation (from single- to multi-domain) in thicker wires.

Acknowledgments J. Liu and J. L. Duan acknowledge support by National NSF of China (Grant Nos. 10775161, 10805062, 10775162) and the West Light Foundation of Chinese Academy of Sciences, PR China. K. Maaz acknowledges the PCSIR of Pakistan for providing 6 months research fellowship.

References

1. T.R. Kline, M. Tian, J. Wang, A. Sen, M.W.H. Chan, T.E. Mallouk, Inorg. Chem. **45**, 7555 (2006)
2. Y. Xia, P. Yang, Y. Sun, Y. Wu, B. Mayers, B. Gates, Y. Yin, F. Kim, H. Yan, Adv. Mater. **15**, 353 (2003)
3. M. El-Kouedi, C.D. Keating, Nanobiotechnology: concepts, applications and perspectives. (Wiley, 2004), pp. 429–443
4. P. Tartaj, M.D. Morales, V.V. Sabino, J. Phys. D Appl. Phys **36**, R-182 (2003)
5. S.D. Bader, Rev. Mod. Phys. **78**, 1 (2006)
6. C.A. Ross, Annu. Rev. Mater. Res. **31**, 203 (2001)
7. R.W. Wood, J. Miles, T. Olson, IEEE Trans. Magn. **38**, 1711 (2002)
8. T.M. Whitney, P.C. Searson, J.S. Jiang, C.L. Chien, Science **261**, 1316 (1993)
9. S. Basu, S. Chatterjee, M. Saha, M. Bandyopadhyay, K. Mistry, K. Sengupta, Sens. Actuat. B Chem. **79**, 182–185 (2001)
10. G. Meng, A. Cao, J.Y. Cheng, A. Vijayaraghavan, Y.J. Jung, M. Shima, P.M. Ajayan, J. Appl. Phys. **97**, 064303 (2005)
11. L. Vila, P. Vincent, L.D.-D. Pra, G. Pirio, E. Minoux, L. Gangloff, S. Demoustier-Champagne, N. Sarazin, E. Ferain, R. Legras, Nano Lett. **4**, 521 (2004)
12. J.U. Cho, J.-H. Wu, J.H. Min, S.P. Ko, J.Y. Soh, Q.X. Liu, Y.K. Kim, J. Magn. Magn. Mater. **303**, e281 (2006)
13. G.J. Strijkers, J.H.J. Dalderop, M.A.A. Broeksteeg, H.J.M. Swagten, W.J.M. de Jonge, J. Appl. Phys. **86**, 5141 (1999)
14. M.A. Kashi, A. Ramzani, A. Khayyatian, J. Phys. D Appl. Phys. **39**, 4130 (2006)
15. M. Darques, L. Piraux, A. Encinas, IEEE Trans. Magnet. **41**, 3415 (2005)
16. Y. Ren, Q.F. Liu, S.L. Li, J.B. Wang, X.H. Han, J. Magn. Magn. Mater. **321**, 226 (2009)
17. G. Ali, M. Ahmad, J.I. Akhter, K. Maaz, S. Karim, M. Maqbool, S.G. Yang, IEEE Trans. Nanotechnol. **9**(2), 223 (2010)
18. S. Karim, W. Ensinger, T.W. Cornelius, E.U. Khan, R. Neumann, J. Nanosci. Nanotech. **8**, 5659 (2008)
19. M.E. Toimil-Molares, V. Buschmann, D. Dobrev, R. Neumann, R. Scholz, I.U. Schuchert, J. Vetter, Adv. Mater. **13**, 62 (2001)
20. C.R. Martin, Science **266**, 1961 (1993)
21. I.U. Schuchert, M.E. Toimil-Molares, D. Dobrev, J. Vetter, R. Neumann, M. Martin, J. Electrochem. Soc. **150**, C189 (2003)
22. W. DeSorbo, Nucl. Tracks **3**, 13 (1979)
23. C. Schönenberger, B.M.I. van der Zande, L.G.J. Fokkink, M. Henny, C. Schmid, M. Krueger, A. Bachtold, A. Huber, H. Birk, U. Staufer, J. Phys. Chem. B **101**, 5497 (1997)
24. S. Karim, M.E. Toimil-Molares, F. Maurer, G. Miehe, W. Ensinger, J. Liu, T.W. Cornelius, R. Neumann, Appl. Phys. A **84**, 403 (2006)
25. E. Ferain, R. Legras, Nucl. Instrum. Methods Phys. Res. B **174**, 116 (2001)
26. P.Y. Apel, I.V. Blonskaya, O.L. Orelovich, S.N. Akimenko, B. Sartowska, S.N. Dmitriev, Colloid J. **66**, 725 (2004)
27. F. Maurer, J. Bröetz, S. Karim, M.E. Toimil-Molares, C. Trautmann, H. Fuess, Nanotechnology **18**, 135709 (2007)
28. X.W. Wang, G.T. Fei, X.J. Xu, Z. Jin, L.D. Zhang, J. Phys. Chem. B **109**, 24326 (2005)
29. E.C. Stoner, E.P. Wohlfarth, Philos. Trans. R Soc. London **A240**, 599 (1948)
30. A. Mumtaz, K. Maaz, B. Janjua, S.K. Hasanain, M.F. Bertino, J. Magn. Magn. Mater. **313**, 266 (2007)
31. R. Ferré, K. Ounadjela, J.M. George, L. Piraux, S. Dubois, Phys. Rev. B **56**, 14066 (1997)
32. J. Duan, J. Liu, T.W. Cornelius, H. Yao, D. Mo, Y. Chen, L. Zhang, Y. Sun, M. Hou, C. Trautmann, R. Neumann, Nucl. Instrum. Methods Phys. Res. B **267**, 2567 (2009)
33. M. Darques, A. Encinas, L. Vila, L. Piraux, J. Phys. D Appl. Phys. **37**, 1411 (2004)